

Corrosion of Depleted Uranium in an Arid Environment: Soil-Geomorphology, SEM/EDS, XRD, and Electron Microprobe Analyses

BRENDA J. BUCK

AMY L. BROCK

Department of Geoscience
University of Nevada Las Vegas
Las Vegas, NV, USA

WILLIAM H. JOHNSON

Department of Health Physics
University of Nevada Las Vegas
Las Vegas, NV, USA

APRIL L. ULERY

Department of Agronomy and Horticulture
New Mexico State University
Las Cruces, NM, USA

Corrosion of anthropogenic uranium in natural environments is not well understood, but is important for determining potential health risks and mobility in the environment. A site in the southwestern United States contains depleted uranium that has been weathering for approximately 22 years. Soil-geomorphic, SEM/EDS, XRD, and electron microprobe analyses were conducted to determine the processes controlling the uranium corrosion. Schoepite and metaschoepite are the primary products of corrosion, and occur as silica-cemented, mixed schoepite-metaschoepite/clay/silt aggregates, as schoepite/metaschoepite-only aggregates, or rarely as coatings upon soil grains. Current extraction procedures do not adequately explain the behavior of uranium in alkaline soils when amorphous silica and clay coatings are present. Soil geomorphology and chemistry at this site limit uranium mobility and decreases potential health risks. However, if land-use and/or regional climate changes occur, uranium mobility could increase.

Keywords Schoepite, metaschoepite, arid soils, sulfate, amorphous silica.

This work was funded by the Environmental Assessment Division of Argonne National Laboratory through a contract with the US Navy Facilities Engineering Command. Thanks to two anonymous reviewers for helpful suggestions to an earlier manuscript, Robyn Howley for field assistance, James Talbot of K/T GeoServices and Nancy McMillan, NMSU for XRD assistance, and Gus P. Williams provided the field photographs.

Address correspondence to Brenda J. Buck, Department of Geoscience, 4505 Maryland Parkway, Las Vegas, NV 89154-4010, USA. E-mail: buckb@unlv.nevada.edu

Introduction

Understanding the behavior of uranium in unsaturated environments is becoming increasingly important because of the planned disposal of nuclear waste in Yucca Mountain Nevada (USA), and the use of depleted uranium (DU) ammunition in recent international conflicts, including: 1991 Iraq/Kuwait (Gulf War I), 1995 Bosnia/Herzegovina, 1999 Kosovo/Serbia, and most recently in 2003 Iraq (Gulf War II) (Bleise *et al.*, 2003). In addition to the military use of DU, non-military uses include radiation shielding in hospitals, a fluorescent additive for now-discontinued porcelain crowns, and in construction of stabilizers for boats and airplanes (Bleise *et al.*, 2003). DU differs from naturally occurring uranium in that it is depleted in ^{235}U and ^{234}U compared to natural uranium. Because ^{235}U and ^{234}U have much shorter half-lives (i.e., more radioactive) than ^{238}U , DU has a lower radiotoxicity than natural uranium, however DU shares the same chemotoxicity with natural uranium (Bleise *et al.*, 2003). The greatest hazards of DU to human and animal populations occur when it is ingested either through inhalation or within drinking water (contamination of aquifers).

The risk of ingesting DU in the environment depends on the amount, chemical composition, and the geologic environment in which it is placed. In the near-surface environment, a soil's chemical and physical characteristics, including pH, redox potential (Eh), cation exchange capacity, (CEC), pCO_2 , amount and type of dissolved solutes, organic matter, porosity, and permeability control its behavior and distribution (Langmuir, 1978). Sorption of uranium onto clays or other mineral surfaces can impede its mobility in sediments. In reducing environments, uranium (IV) is generally insoluble. In oxidizing conditions however, uranium corrodes rapidly, forming U(VI) compounds that for the most part, are fairly soluble and mobile (Meinrath *et al.*, 2003). In unsaturated soil U(VI) in the presence of arsenates, vanadates, silicates and phosphates, forms insoluble minerals (Langmuir, 1978). If these ligands are not available, hydrolysis and carbonate complexes (especially at alkaline pH) are formed that can be mobile (Elless *et al.*, 1997; Meinrath *et al.*, 2003). Therefore, in determining the mobility, bioavailability, and toxicity of uranium contamination, it is very important to understand the physical and chemical characteristics of the contaminated soils (Figueiras *et al.*, 2002; Elless and Lee, 2002), and associated uranium minerals.

Despite the importance of determining environmental risks, identification of these minerals can be difficult. Scanning electron microscopy (SEM) with energy dispersive spectrometry (EDS) is not accurate in identifying elements with low atomic numbers. Therefore, carbonate and oxide compounds cannot be differentiated. In addition, the use of coating materials in sample preparation can mask some peaks or cause others to overlap. Some of these problems can be overcome using X-ray diffraction (XRD) and electron probe microanalysis (EPMA) for mineral phase identification of the same samples. For XRD analyses to be effective, fine-grained secondary uranium minerals must be crystalline or have at least short-range order and need to be separated from the surrounding soil grains through density fractionation (Elless *et al.*, 1997). Irreversible dehydration of schoepite at room temperatures also makes its identification difficult by XRD (Wronkiewicz *et al.*, 1992). Backscatter electron analysis as part of EPMA can aid in phase identification based upon the relative proportion of elements present in the mineral phases of interest. Also, EDS may be used to calculate elemental composition of minerals within an error of $\pm 1\%$. Electron microprobe analyses are even more accurate (e.g., $\pm 0.1\%$). Combining results from multiple analytical techniques increases the potential for accurate identification and interpretations.

Despite the fact that two of the four recent international conflicts (Gulf War I and II) and the proposed Yucca Mountain nuclear waste storage site occur in arid environments,

very few studies have concentrated on the behavior of uranium in arid soils. Because of the lack of water, high pH, and increased potential for carbonate complexation in most arid systems, we hypothesize that predicting uranium mobility is best achieved by determining dissolution/precipitation chemistry and mineralogy rather than measuring uranium sorption/desorption through distribution coefficients (K_d). In this study, SEM/EDS, XRD, and microprobe analyses of weathered anthropogenic uranium were studied at two sites in the Mojave Desert. The results indicate that movement of the uranium into the soil occurs primarily through dissolution and re-precipitation of uranium oxides.

Methods

A 1 km² site in the southwestern United States contained DU penetrator that had been weathering in the soil for approximately 22 years. This site was mapped using aerial photography, field reconnaissance, and analysis of soil profiles (Figure 1). Five soil profiles were excavated, described and sampled according to the USDA NRCS Field Book for Describing and Sampling Soils (Schoeneberger *et al.*, 1998). All soil colors were measured using the Munsell Soil Color chart on moist samples. Calcium carbonate and organic matter was removed and soil texture (hydrometer method) was determined using methods described by Gee and Bauder (1986). Particle density, total porosity and volumetric water content were measured using guidelines from Palmer and Troeh (1995). Organic carbon content was determined using removal by hydrogen peroxide (Gee and Bauder, 1986). An Accumet Basic Conductivity Meter and VWR model 8100 pH meter were used on a 1:1 paste to determine electrical conductivity and pH on two soil profiles adjacent to corroded DU penetrators. The above analyses were conducted at the UNLV Pedology Lab. Cation exchange capacity (CEC) was determined using the NaOAc/NH₄OAc replacement method at the Utah State University Analytical Laboratory (Rhoades, 1982).

Two locations, KS01 and KS05 (see Figure 1), contained a DU penetrator at the surface. At these sites, horizontal and vertical soil samples were collected to determine uranium

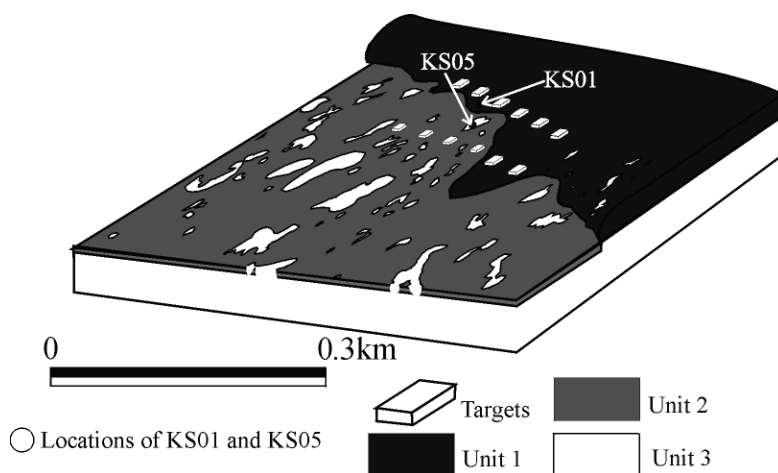


Figure 1. Soil map of study area with vertical exaggeration. Unit 1 is characterized by thick (20–50 cm) Holocene eolian sand overlying coarse Pleistocene beach deposits. Unit 2 is characterized by Holocene eolian sand of variable thickness (1–10 cm) overlying fine silty Pleistocene lake deposits, and Unit 3 is characterized by eolian blowout depressions exposing Pleistocene fine-grained lake deposits, commonly containing salt crusts at the surface.

movement (Johnson *et al.*, 2004). The vertical samples were analyzed in detail using a light microscope, SEM equipped with an EDS, an EPMA equipped with wavelength dispersive spectrometers (WDS) at the UNLV EMIL lab; and XRD analyses at the New Mexico State University Mineralogy Lab and K/T Geoservices Inc. Additionally, surface salt crusts at site KS05 were scraped from the surface, placed in plastic containers and similarly analyzed because the mineralogy, quantity and location of the salts were expected to influence possible uranium migration. For XRD analyses, no sample prep was performed on the samples. Vaseline and/or double-sticky tape were used to adhere the samples to the 25 mm glass microscope slide to promote random orientation. XRD analyses were performed on a Rigaku automated powder diffractometer using $\text{CuK}\alpha$ (0.15418 nm) radiation at power settings of 40 kV and 35 mA and a monochromatic scintillation detector. The samples were analyzed over an angular range of 2–65 degrees 2 theta at a rate of one degree per minute. Because both initial SEM and XRD analyses of the uranium minerals were difficult in these mixed soil samples, the uranium precipitates and uranium coated soil particles were separated from the soil samples through heavy liquid separation using bromoform (specific gravity = 2.89 g/cm^3) (Klein and Hurlbut, 1993). To prevent the loss of any uranium materials, the lighter materials were examined with a microscope prior to discarding. The heavier materials were washed with acetone, air-dried, mounted, and sputtered with gold (for SEM analyses) or carbon (for EPMA). 522 SEM (BSE) images, 461 EDS analyses, and 20 EPMA/WDS maps were used to examine the morphologies and chemical compositions of the uranium precipitates as they occur in the soil as well as their association with other soil particles and minerals.

Results

Site Soil-Geomorphology Characteristics

Lower elevations in the southwestern United States are characterized by hot, arid climates, often with little to no vegetation. Many of the intrabasinal areas contain now-dry lake beds (playas) that were fresh or salt-water lakes during the Pleistocene. Our study site is located along the northern shoreline of one of these playas. The modern topography is a result of Holocene and modern eolian and minor fluvial reworking of the Pleistocene lake sediments. These are composed primarily of coarse-grained sandy to pebbly beach deposits, and fine-grained playa and lacustrine clays with associated salts. Two rows of targets were placed at this location and DU ammunition was fired at these targets approximately 22 years ago. The upper row of targets is located at a topographically higher position atop the Pleistocene beach deposit. The second row of targets is located topographically lower within the playa/lacustrine sediments (Figure 1).

Within this 1 km^2 study area, five soil profiles were excavated and described. Three soil-geomorphic units were identified and mapped to determine the surface and soil variability within the study site and to predict uranium behavior in these sediments (Figure 1). Unit 1 is a Pleistocene beach deposit covered with young (late Holocene to modern) fine to medium eolian sand. The thickness of this sand (C horizon) varies with location along the berm. Unit 2 is composed of a thin veneer of fine to medium eolian sand (same as above) that overlies fine-grained Pleistocene lake deposits. The thickness of this unit varies greatly throughout the study area. The primary controls on its thickness are prevailing wind directions, the position and type of vegetation, target location, ruts created by vehicle traffic during wet periods, and proximity to the Pleistocene beach berm (Unit 1) where the thickest deposits of this sand are draped. Unit 3 is composed of eolian deflation areas where the fine-grained Pleistocene lake deposits are exposed at the surface. This surface is characterized

by fine-grained lacustrine sediment with salt crusts and mudcracks. The depressions are periodically flooded and can contain standing water. Soil characteristics suggest that the water table lies very close to the surface. Seasonally, the depth to the water table can vary between 0 and 59 cm as evidenced by mottling and low chromas. This depth primarily depends upon the thickness of the overlying Holocene eolian sand.

Two soil profiles (KS01 and KS05) were excavated in April 2002 adjacent to two surficial DU penetrators to determine the soil properties that affect uranium migration (Table 1). KS01 is located along the beach berm in Unit 1. Additional information regarding these penetrators and the horizontal and vertical uranium distribution can be found in Johnson *et al.* (2004). KS01 is characterized by a 2.5Y 6/3 (light yellowish brown), coarse-grained, C horizon (0–25 cm) overlying a partially cemented Btk horizon (25–33 cm) containing clay skins and pedogenic carbonate. The surficial C horizon is composed of stratified medium to coarse sand that in places is weakly cemented with salts. At the time of the excavation, the underlying Btk horizon was moist and contained fine horizontal roots. This horizon is violently effervescent, 5Y 6/4 (pale olive) sandy loam, fining upward with poor sorting at the top, grading to well sorted coarse sandy loam at its base. Beneath this horizon is a buried soil consisting of 2A1 (33–45 cm), 2A2 (45–59 cm) and 2Bg (59–67 cm) horizons. The 2A1 and 2A2 horizons differ in that 2A1 contains a greater amount of clay (clay loam) coating the coarse sand grains and is slightly more indurated. The 2A2 horizon contains coarser sand and pebbles (sandy loam) and the clay coatings are found mostly underneath the grains as pendants. Both are violently effervescent and are also partially cemented with clay, salts, and organic matter films around grains. The 2A1 horizon has moist colors of 2.5Y 3/2 (very dark grayish brown) and 5Y 3/2 (dark olive gray), and the underlying 2A2 horizon is 5Y 3/2 (dark olive gray). The 2Bg horizon is a non-effervescent, 5Y 5/4 (olive), well-sorted sandy loam containing mottles rimmed with hematite stains. Soil pH values are lowest at the surface (9.2) and increase with depth (10.4) (Table 1). Electrical conductivity, indicating increased salt content, is greatest in the Btk and 2A1 horizons (Table 1). The greatest uranium K_d values (140 L/kg) were in the 2A1 horizon (Johnson *et al.*, 2004), which also has the highest CEC values.

Near the KS01 soil profile, the DU penetrator at the surface was bright yellow (2.5Y 8/8) and visibly corroded. Radioactive, yellow particles were present at the soil surface and beneath the penetrator in a cone-shaped pattern narrowing with increasing depth (Figure 2a). Distinct large yellow particles cementing soil particles occurred from the surface to a depth of 4 cm. Beginning at 2.5 cm, but becoming dominant at 4 cm, a white cementing mineral that visually appeared to be pedogenic calcium carbonate (stage II) formed a 1 cm thick layer. This layer continued to 8 cm depth with decreasing cementation in a cone-shaped pattern (Johnson *et al.*, 2004) (Figure 2b). Radioactivity of the sediment measured in the field indicated that uranium substances were present to 10 cm depth. The white cementing mineral reacted with dilute HCl under a light microscope and is inferred to be calcium carbonate. Uranium samples at this site were also analyzed under a light microscope. The uranium particles were friable, with a bright to pale yellow color (2.5Y 8/8, 7/8, 8/4; 5Y 8/8), and had either a glassy or vitreous luster.

The second soil profile, KS05, is located within Unit 3 in an eolian blowout depression (Figure 1). This soil is developed within the Pleistocene lake deposits. It is characterized by a thin A horizon (0–2 cm) overlying a partially cemented Btkz horizon (2–7 cm) followed by three By horizons (Table 1). The surface of the A horizon contains numerous mudcracks, salt crusts, and mica. It has a strong platy to strong medium subangular blocky structure, is 5Y 6/3 (pale olive) in color, and is a violently effervescent loam. The underlying Btkz horizon (2–7 cm) is a violently effervescent loam, with strong coarse to medium subangular

Table 1
Soil physical and chemical data

Profile ID	Depth (cm)	Color moist	pH	Electrical conductivity ($\mu\text{S}/\text{cm}^2$)	O.M. %	CEC (meq/100 g)	Texture	Structure
KS01								
KS01-C-NG	1-25	2.5Y 6/3	9.2	6.4	0.004	1.5	Loamy sand	Single grain
KS01-Btk-NG	25-33	5Y 6/4	10.2	1.9	0.036	6.8	Sandy loam	Single grain
KS01-2A1-NG	33-45	2.5Y 3/2 5Y 3/2	10.2	2.7	0.054	28.6	Clay loam	Strong, coarse, subangular blocky
KS01-2A2-NG	45-59	5Y 3/2	10.4	1.3	0.004	13.3	Sandy loam	Strong, medium-coarse, subangular blocky
KS01-2Bg-NG	59-67	5Y 5/4	10.3	1.7	0.000	6.2	Sandy loam	Weak, single grain
KS05								
KS05-A-NG	0-2	5Y 6/3	8.6	27.3	0.077	9.1	Loam	Strong, medium subangular blocky-platy
KS05-Btkz-NG	2-7	5Y 6/3	10.1	18.6	0.022	12.7	Loam	Strong, medium-coarse, subangular blocky
KS05-By1-NG	7-19	5Y 5/3	9.9	7.8	0.008	5.2	Sandy clay loam	Moderate, medium, subangular blocky-platy
KS05-By2-NG	19-33	5Y 7/3	9.4	7.1	0.037	5.5	Loam	Moderate, coarse-medium, subangular blocky
KS05-By3-NG	33-60	5Y 7/3 5Y 6/3	8.9	3.9	0.004	4.7	Sandy loam	Moderate, medium, subangular blocky

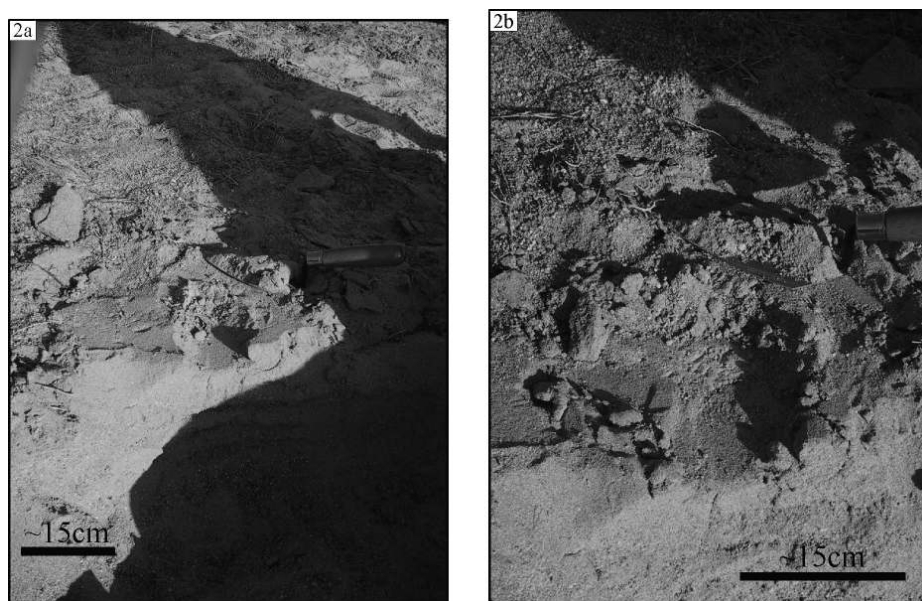


Figure 2. Corroded DU penetrators at site KS01: (a) yellow schoepite/metaschoepite at 2.5 cm depth; (b) white calcium carbonate at 4 cm depth.

blocky structure, 5Y 6/3 (pale olive color), and has pores (1–4 mm) coated with pedogenic salts, amorphous silica, and clay. The underlying By1 horizon (7–19 cm) is a sandy clay loam, strongly effervescent, with moderate medium subangular blocky to platy structure, 5Y 5/3 (olive) in color, and contains stage I gypsum snowballs (Buck and Van Hoesen, 2002). The By2 (19–33 cm) shows an increase in the morphologic state of development of the pedogenic salts with gypsum snowballs and rare incipient state II gypsum nodules, which give it a slightly lighter color, 5Y 6/3 (pale olive) (Buck and Van Hoesen, 2002). This horizon has numerous root casts 3–5 mm wide by 1 cm in length coated with salts, a moderate coarse to medium subangular blocky structure, is violently effervescent, and is a sandy loam. The By3 horizon (33–60 cm) contains gypsum snowballs and stage II nodules 1–3 cm in diameter, has a moderate medium angular blocky structure, and 5Y 7/3 (pale yellow), 5Y 6/3 (pale olive) colors, is violently effervescent, and is a sandy loam. Soil pH varied throughout this profile between 8.5 and 10, with the highest pH and CEC occurring in the Btkz horizon (Table 1). The greatest amount of salt occurs at the surface, and in the underlying Btkz horizon as indicated by EC (Table 1). The Btkz horizon (2–7 cm) has one of the highest calculated K_d values (110 L/kg) (Johnson *et al.*, 2004). The weathered DU penetrator at this site was black and not as corroded as at site KS01. Uranium fragments were found in an adjacent mudcrack, but no visual evidence during field collection for either horizontal or vertical uranium movement beyond that was found (see also Johnson *et al.*, 2004). Concentrated uranium particles were examined under a light microscope and were friable, 5Y 8/8, (yellow), and vitreous.

Laboratory Analyses

SEM/EDS analyses of the salt crusts at site KS05 indicate that they are composed of halite (NaCl), mirabilite ($\text{Na}_2\text{SO}_4 \cdot 10\text{H}_2\text{O}$) and/or thenardite (Na_2SO_4), gypsum ($\text{CaSO}_4 \cdot 2\text{H}_2\text{O}$),

Table 2
XRD results

Sample and Depth (cm)	Halite	Thenardite	Schoepite	Metaschoepite	Amphibole
KS01					
1–3			X	X	X
3–4				X	X
4–5				X	
5–6					X
6–8	—	—	—	—	—
8–10	X				X
KS05					
0				X	X
0–3				X	X
3–6	—	—	—	—	—
KSO5 surface salts	X	X			X

eugsterite ($\text{Na}_4\text{Ca}(\text{SO}_4)_3 \cdot 2\text{H}_2\text{O}$) and/or glauberite ($\text{Na}_2\text{Ca}(\text{SO}_4)_2$). Halite and thenardite were identified through XRD analysis (Table 2). Halite occurs as subhedral to anhedral cubic crystals ranging from 10–20 μm in size (Figure 3a). Evidence for mirabilite and/or thenardite is distinct S and Na EDS peaks (Figure 3b). SEM evidence for mirabilite is its 4–7 μm , subhedral tabular crystal habit (Figure 3a–c). Thenardite was identified by XRD d-spacings of 2.78, 3.18, and 4.64 (Table 2), and 1–5 μm euhedral acicular crystals in SEM analysis. Mirabilite is the hydrated form of sodium sulfate and is more stable than thenardite in cooler temperatures and higher relative humidities (Driessen and Schoorl, 1973; Wiedemann and Smykatz-Kloss, 1981; Keller *et al.*, 1986; Timpson *et al.*, 1986). Thus, it was not surprising that mirabilite was found in the surface crust sampled in April. The presence of either of these minerals could have been the result of dissolution/re-precipitation of either phase during transport and laboratory analysis because slight changes in humidity and temperature can cause their hydration/dehydration (Keller *et al.*, 1986). Evidence for eugsterite and/or glauberite was weak by XRD and may have been masked by other minerals. However, characteristic Na-Ca-sulfate signatures on SEM/EDS coupled with distinctive crystalline morphology were indicative of the presence of these rare salts (Skarie *et al.*, 1986).

Laboratory analyses at both KS01 and KS05 sites show that uranium occurs as precipitates of uranium oxides within soil pore spaces. SEM/EDS results show tabular pseudo-hexagonal crystals composed of 60 to 95% uranium. These crystals are found in aggregates of clay and silt coated and cemented with amorphous silica, aggregates of uranium oxide crystals without the clay and silica cements, or rarely as a precipitated coating on soil grains (Figures 3d–h and 4a–f). The uranium oxides resulting from corrosion of the DU penetrators were in far lower concentration than other soil minerals and were difficult to detect with XRD. Heavy liquid separation helped concentrate the uranium minerals for XRD analyses. Schoepite and metaschoepite were identified as the uranium oxide minerals by comparison to reference standards. The primary d-spacings for identifying schoepite are 7.35, 3.66, 3.24, and 2.45. Metaschoepite's most intense d-spacings are 7.35, 3.59, 3.22, and 3.16. Schoepite was found at KS01, 1.3–2.5 cm depth (size fraction between 53 and 125 μm), and metaschoepite in all depths at KS01 except 8 to 10 cm, which did not have

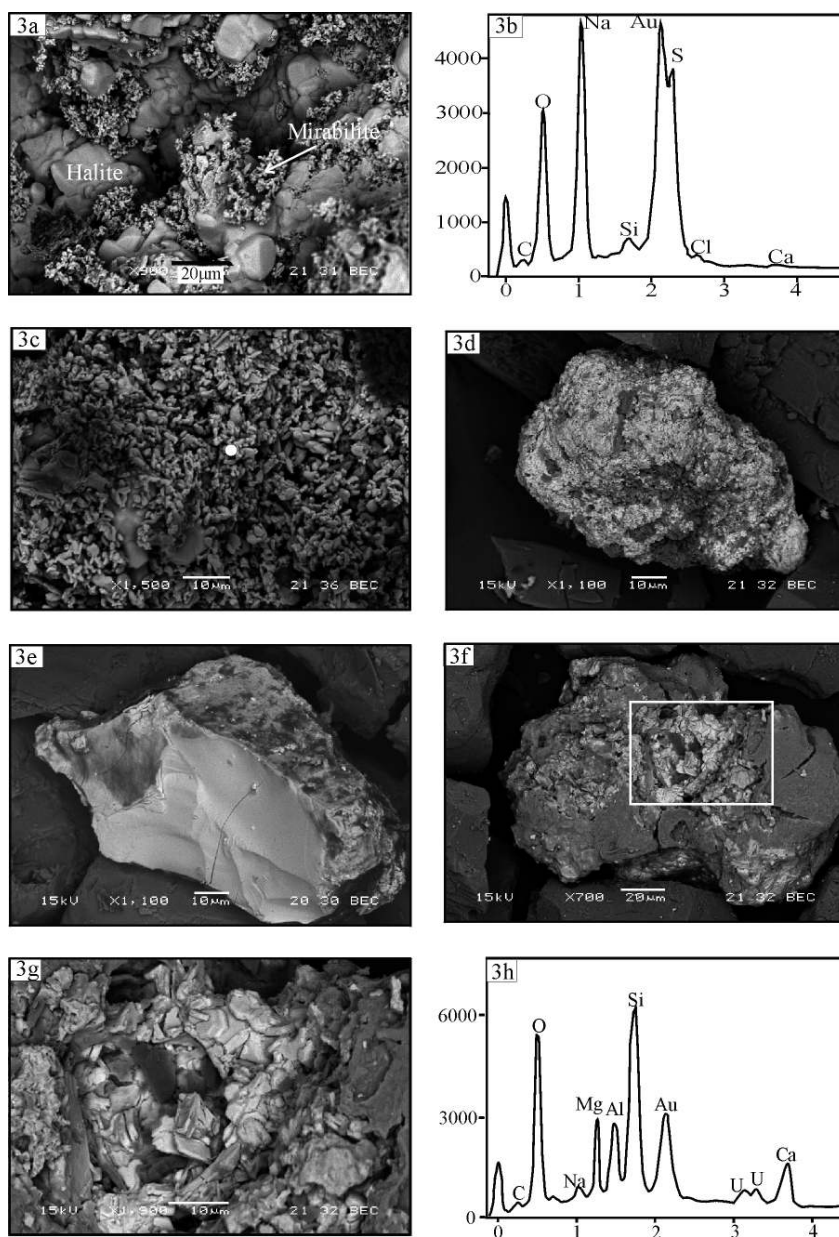


Figure 3. (a) SEM backscatter image of KS05 surface salts halite and mirabilite. (b) EDS analysis of salts in 3c indicating Na-sulfate. (c) SEM backscatter image of mirabilite/thenardite. White dot shows location of EDS analysis shown in 3b. (d) SEM backscatter image of aggregate of amorphous silica/clay/silt (grey) and schoepite/metaschoepite (white) from KS01 6–8 cm depth. (e) SEM backscatter image of schoepite/metaschoepite precipitate coating quartz grain from KS01 5–6 cm depth. (f) SEM backscatter image of aggregate of amorphous silica/clay/silt and schoepite/metaschoepite from KS01 3–4 cm depth. (g) Close-up SEM backscatter image of white box outlined in 3f. Euhedral, pseudo-hexagonal, tabular schoepite (white) in clay/silt aggregate coated with amorphous silica (grey). (h) EDS analysis of clay/silt showing Si and Al peaks. Au peak is a result of the gold coating used in sample preparation.

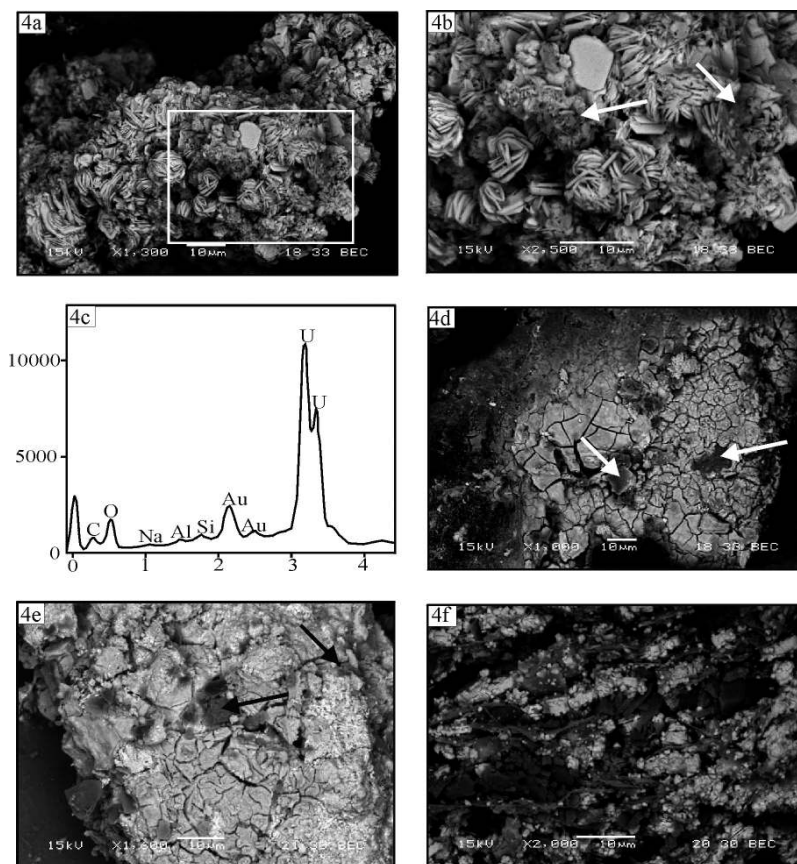


Figure 4. (a) SEM backscatter image of tabular, pseudo-hexagonal rosettes of schoepite from KS01 3–4 cm depth. (b) Close-up SEM backscatter image of white box in 3a. White arrows show amorphous silica coatings and clay/silt particles. (c) EDS analysis of schoepite/metaschoepite. (d) SEM backscatter image of metaschoepite with desiccation cracks at KS01 3–4 cm depth. White arrows show amorphous silica coatings and clay/silt particles. (e) SEM backscatter image of schoepite/metaschoepite at KS01, 0–3 cm depth (size fraction between 53 and 125 μm). Metaschoepite displays desiccation cracks. Arrows point to amorphous silica coatings and clay/silt particles. (f) SEM backscatter image of schoepite precipitated within mica sheets at KS01, 0–3 cm depth (size fraction between 53 and 125 μm).

sufficient recoverable uranium materials to analyze by XRD (Table 2). At KS05, only the surface sample had sufficient uranium material to analyze by XRD and was identified as metaschoepite. SEM/EDS techniques, however, were able to analyze uranium materials at all sampled depths. Uranium is found as either (1) aggregates of amorphous silica-cemented schoepite/metaschoepite/clay/silt, (2) aggregates of schoepite/metaschoepite crystals-only, and (3) schoepite/metaschoepite coatings on soil grains. The distribution of these three types of uranium mineral occurrence (Figure 5), grain size (Tables 3 and 4), crystal habit (Tables 3 and 4), and amount of dehydration (metaschoepite) vary with depth (Figure 5). Metaschoepite is distinguished from schoepite by numerous desiccation cracks caused by the volume decrease during dehydration (Figure 4d–e). EPMA element scans for U, Ti, Si and Al show an elevated concentration of uranium in the center of the aggregates.

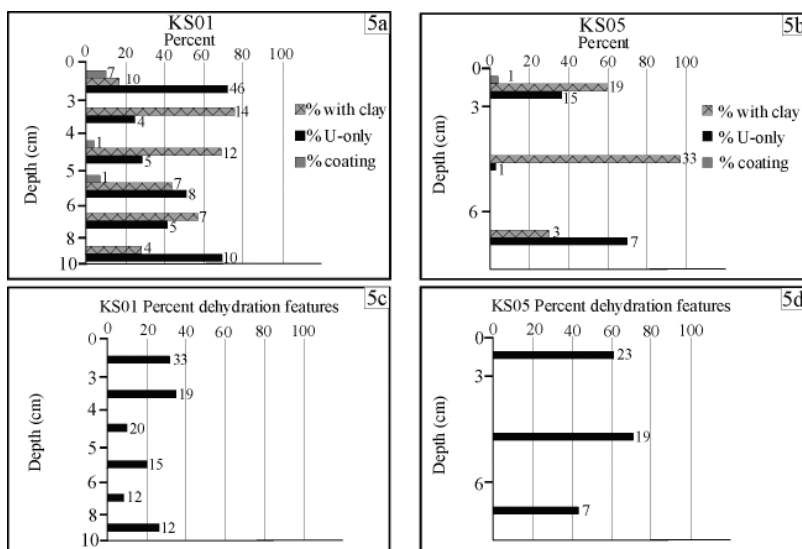


Figure 5. (a) KS01 percent occurrence of uranium precipitates with depth. (b) KS05 percent occurrence of uranium precipitates with depth. Hatched pattern indicates percent uranium minerals occurring as aggregates with clay and amorphous silica as shown in Figure 3f. Uranium minerals indicated by the black bars are similar to those shown in Figure 4a, and gray bars to those shown in Figure 3e. (c) KS01 percent of uranium minerals containing dehydration features with depth. (d) KS05 percent of uranium minerals containing dehydration features with depth. Numbers at end of bars represent total observations.

Titanium was found in association with uranium in a few samples. In contrast, aluminum and silicon are concentrated along the outer rim of aggregates, surrounding the uranium, and not chemically bound with it (Figure 6). EDS and backscatter analyses also show these chemical relationships (Figures 3d–h and 4a–f).

Table 3
Uranium crystal habits and size at site KS01

Depth (cm)	Size range (μm)	Crystal habit
1–2.5	1–15	Euhedral to subhedral, tabular, rectangular and pseudo-hexagonal, books and rosettes
2.5–4	1–20	Euhedral tabular books
	5–50	Subhedral and anhedral massive
4–5	1–10	Euhedral to subhedral, tabular rectangular and pseudo-hexagonal, books and rosettes
5–6	1–5	Subhedral to euhedral tabular, rectangular and pseudo-hexagonal
6–8	1–5	Subhedral to euhedral tabular rectangular and pseudo-hexagonal
	5–50	Anhedral massive
8–10	1–5	Euhedral, tabular, hexagonal
	5–20	Anhedral massive

Table 4
Uranium crystal habits and size at site KS05

Depth (cm)	Size range (μm)	Crystal habit
0	Bimodal 1–3; 5–10	Euhedral to subhedral tabular, rectangular and pseudo-hexagonal books and rosettes
	5–300	Anhedral massive
0–2.5	1–5	Subhedral to euhedral tabular, rectangular and pseudo-hexagonal books
	5–10	Anhedral massive
2.5–6	3–7	Anhedral massive
	1–5	Euhedral to subhedral tabular, rectangular and pseudo-hexagonal books

Discussion

Health risks associated with DU ammunition are proportional to its potential for redistribution through air and water—either as fine particulate matter suspended within the atmosphere or through its solubilization and contamination of groundwater aquifers (Bleise *et al.*, 2003). The results of this and the parallel study of Johnson *et al.* (2004) indicate that both of these potential exposure pathways are low at this site.

Although eolian processes dominate sediment movement at the study site, there was little evidence of horizontal movement of DU particulates at this site. Soil-geomorphological results indicate that overland runoff is predicted to occur during intense precipitation events moving some sediment (and potentially DU particulates) from the topographically higher Pleistocene beach berm into the lower eolian deflationary depressions (Figure 1). These depressions lie primarily in the southern portion of the study area. Ponding of water in these depressions is caused by low permeability of the fine-grained lake sediments. This ponding could contribute to the lateral spreading of uranium contaminants; however, no evidence was found to support this. Locally, the water table is shallow, at times at the surface within the lower margins of the playa. Overall, the characteristics of the soils at the study site are controlled by the different sedimentary facies of the now-dry Pleistocene lake with minor Holocene and modern eolian modifications.

Characterization of soil profile KS01 indicates the presence of a periodically perched water table caused by the semi-indurated Btk horizon at 33 cm. The depth to this horizon varies within Unit 1, but the presence of water at the time of excavation, abundant horizontal roots, and the evidence of previously ponded water at this depth indicated by salt cementation, suggests a seasonally perched water table above this horizon in the study area. In addition, the 2A1 horizon beneath this layer contains significantly more clay and has higher EC values, indicating that downward moving water is severely restricted through these two horizons (Table 1). The mottled and non-effervescent character of the 2Bg horizon at the base of KS01 indicates that this horizon is at least seasonally saturated and is representative of the regional water table. Uranium movement within Unit 1 would be predicted to be minimal beyond the Btk or 2A1 horizons because of their semi-indurated nature, and increased CEC, salt, and organic matter contents (Table 1). Any uranium minerals that did not precipitate out of solution at this depth are predicted to be sorbed onto cation exchange sites of the clays and organic colloids. Sorption/desorption results of Johnson *et al.* (2004) support these predictions.

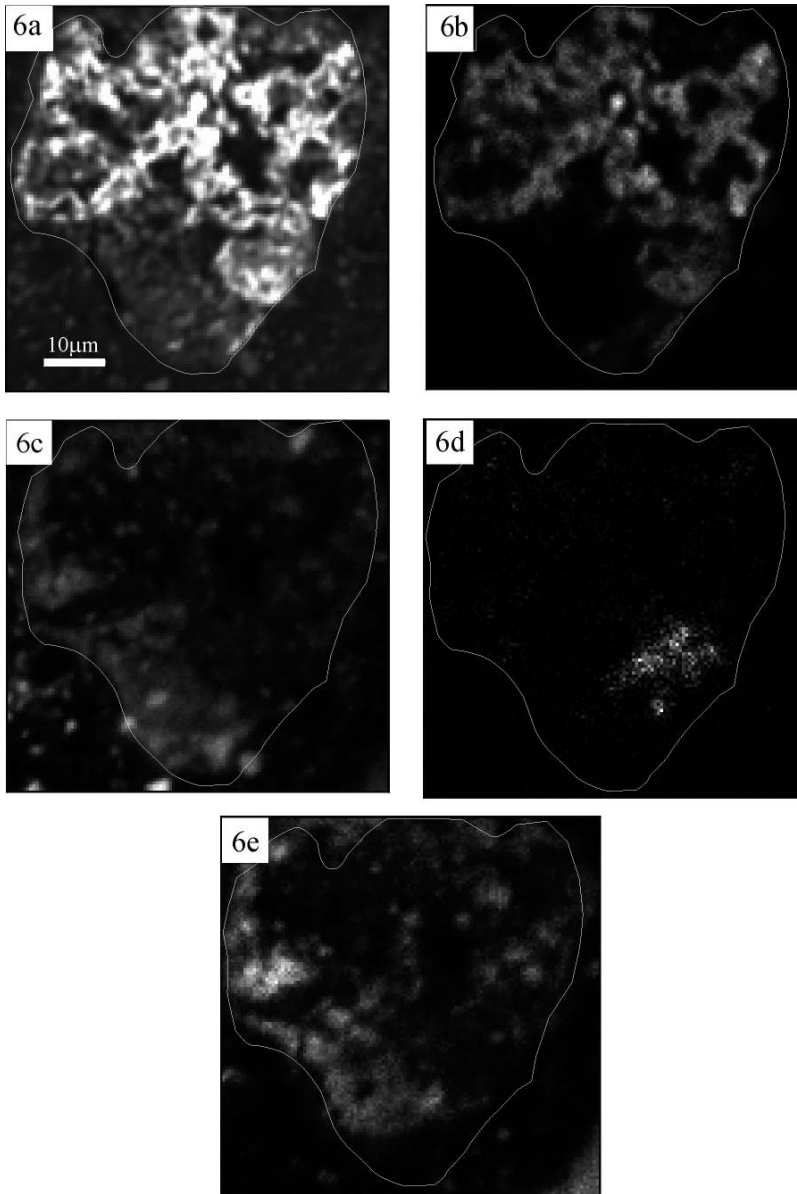


Figure 6. EPMA map scan of amorphous silica coated, schoepite-metaschoepite/clay/silt aggregate from KS01, 5–6 cm depth. (a) BSE. (b) Uranium. (c) Silica. (d) Titanium. (e) Aluminum.

In contrast, uranium movement within Unit 3 and at site KS05 will be complicated by the seasonal surficial ponding of water indicated by salt crusts and mudcracks within the eolian blowout depressions. Higher clay content and Na-caused dispersion of the clay particles during seasonal ponding probably causes lower hydraulic conductivity in the underlying Btkz horizon (Table 1). Therefore, water and thus potential uranium mobility through this horizon is restricted. Research by Johnson *et al.* (2004) supports this and also shows increased K_d values within this horizon.

SEM/EDS, XRD, and electron microprobe analyses of uranium-containing soil samples beneath the two weathered DU penetrators indicate that precipitation processes are the dominant mechanism controlling uranium mobility at this site (Figures 3d–h, 4a–f, 6, and Table 2). Vertical movement of the uranium occurs primarily through the processes of dissolution and re-precipitation into new minerals, rather than through translocation or sorption/desorption. This is consistent with results reported by Barnett *et al.* (2000) that showed sorption/desorption processes become less important with increased pH, dissolved carbonate, and increased U(VI)-carbonate complexes. Previous studies in the laboratory or even in humid climates have also found precipitation mechanisms to be more important than previously thought (Elless and Lee, 1998; Murakami *et al.*, 2001; Johnson *et al.*, 2004).

SEM/EDS combined with XRD data show that uranium minerals occur primarily as euhedral to subhedral books and rosettes of tabular pseudo-hexagonal crystals of schoepite and/or as massive, anhedral dehydrated schoepite (metaschoepite) (Tables 3 and 4). SEM images of the metaschoepite show numerous spallation cracks from a decrease in volume during the dehydration of schoepite (Figure 4d–e). Finch and Ewing (1992) suggest that dehydrated schoepite may inhibit the formation of schoepite. Although the results of this study cannot definitively support or deny this statement, XRD and SEM analyses do show an increase in metaschoepite with an accompanying decrease in schoepite (Table 2). Because all of the samples were treated the same during transport and analyses, it is unlikely that this relationship is a product of dehydration of schoepite during analyses.

SEM analyses can be especially useful to interpret the genesis of uranium minerals in soils. The morphology of the rosettes of euhedral schoepite is similar to micro-snowballs of sulfate salts precipitating in other arid soils (Figure 4a–b) (Merkler *et al.*, 2002; Buck *et al.*, 2002). This supports the interpretation of uranium dissolution and re-precipitation caused by rapid soil water evaporation. Some of the schoepite crystals are skeletal (hollow), indicating their formation was the result of supersaturation and rapid precipitation in this arid environment. The increased concentration of calcium carbonate in association with schoepite and metaschoepite beneath the penetrator at KS01 indicates a zone of preferential vertical soil water movement. However, no surface or subsurface soil data such as textural changes or concentrations of root or pore spaces were observed to explain this relationship. Increased desiccation features associated with the volume decrease caused by dehydration of schoepite to metaschoepite were significantly greater in the KS05 site compared to KS01. This may be a function of the numerous seasonal wetting/evaporation episodes that occur in Unit 3. Although dehydration could have also occurred during sample transport and analyses, both KS01 and KS05 samples were treated identically, therefore suggesting the different percentages of dehydration features are a result of localized site characteristics that control soil moisture content.

Amorphous silica and/or authigenic aluminum silicate clays have precipitated around the uranium-oxides (Figures 3d–h, 4a–f, and 6). Silica solubility and illuviation is increased by the high pH of these arid soils. Thus, these materials are common pedogenic products that accumulate in the subsurface of arid soils over time (Chadwick *et al.*, 1989; Monger and Kelly, 2002). These coatings increase significantly with depth in both profiles as illuviation processes become more important (Figure 5). The mixed-aggregate nature of the schoepite and metaschoepite with the clay and silica indicates multiple episodes of both uranium and silica/clay dissolution, downward movement in solution, and reprecipitation within soil pore spaces. Although significant amounts of dissolved silica must at times be in solution with uranium (VI), no evidence of uranyl silicates was found. A laboratory experiment by Sowder *et al.* (1996) found similar results: in the presence of silica, the transformation of schoepite to becquerelite is retarded, and added silica did not cause uranyl silicates to form.

In contrast, Finch and Ewing (1992) found that schoepite alters readily to uranyl silicates. A better understanding of the relationship between uranium corrosion and site-specific factors such duration of weathering, solution chemistry, pH, and temperature is needed.

The behavior of amorphous silica and authigenic clays in relation to the DU in this study is very important. Results in Johnson *et al.* (2004) on these samples indicate that the coatings of amorphous silica and clay affect the solubility of the schoepite and metaschoepite in extraction analyses. Johnson *et al.* (2004) found that the extractable uranium decreased with increasing soil depths, paralleling our results showing increased uranium/clay/silt aggregates coated with amorphous silica and authigenic clays. Therefore, we interpret these extraction results to have been caused by the amorphous silica and clay coatings around the uranium oxides, and not by formation of less-soluble uranyl silicates (Johnson *et al.*, 2004). Thus, there is potential for erroneous interpretations of uranium solubility in arid, alkaline soils when using the current extraction procedures.

Titanium was part of the original DU ammunition used at this site, and is a common component (0.75% by weight) in DU penetrators used in recent conflicts (Giannardi and Dominici, 2003; Pollanen *et al.*, 2003). SEM/EDS and electron microprobe data possibly suggest that the Ti dissolved and re-precipitated in association with the uranium (Figure 6). Electron microprobe mapping suggests that Ti, when present, appears to be associated with the uranium-oxides (Figure 6b, 6d), and not with the associated clays or amorphous silica (Figure 6c, 6e). This behavior was also found in DU ammunition in Kosovo (Danesi *et al.*, 2003). Previous research (Levy *et al.*, 1973) indicates that the presence of Cl significantly aids in the corrosion of anthropogenic uranium containing Ti. At site KS05, the SEM/EDS data indicate that halite (NaCl) is the most abundant salt mineral present (Figure 3a). Seasonal ponding of surface waters, in addition to upward-moving capillary water at this site is predicted to concentrate Cl-bearing solutions causing increased corrosion of the Ti-bearing uranium. Thus, the difference in geomorphic position between site KS01 and KS05 could significantly affect how the anthropogenic uranium in these areas corrodes. However, because soils in arid climates are much more likely to contain salts than those in other climates, caution using Ti-alloyed DU ammunition in arid environments is recommended.

The results of this study indicate that potential risks through dust inhalation or aquifer contamination are currently low at this site. However, changes in land use or regional climate patterns could increase these risks. The very small size of these uranium particles has an increased potential for re-dissolution and/or atmospheric re-suspension and inhalation (Tables 3 and 4). Similar size ranges were found for weathered DU penetrators in Kosovo (Danesi *et al.*, 2003). Surficial disturbances, such as removing vegetation, and/or construction, could disrupt the subsurface horizons that currently are restricting uranium mobility into the regional water table. Additionally, subsurface silica-coated uranium particles could become more soluble through disturbance and dissolution of the silica and/or clay coatings. For these reasons, understanding the soil processes controlling uranium corrosion is essential for proper land-use management and environmental contamination prevention.

Conclusions

Uranium mobility is directly related to local changes in sediment facies resulting from Pleistocene and Holocene lacustrine/playa/beach deposits that have been modified by modern eolian reworking. These geologically controlled parent materials and their resulting local topography impact soil chemistry and water movement, and thus uranium mobility. It is imperative to apply geologic and soil science techniques when estimating the potential transport of DU. The results of this study indicate that DU undergoes dissolution and

re-precipitation into soluble uranium oxides. However, with greater depths, schoepite and metaschoepite are increasingly coated with amorphous silica and/or are found in aggregates with clays. Because of these coatings, currently used extraction procedures may lead to inaccurate interpretations for DU without additional SEM/EDS, XRD, and electron microprobe analyses.

Some evidence for possible Ti mobility associated with the DU penetrators was suggested by SEM/EDS and electron microprobe analyses. Geomorphic location within the study area may control the corrosion rate of Ti-alloyed DU penetrators, as increased Cl concentrations associated within seasonally-ponded depressions may increase their corrosion rate. However, the arid climate, semi-indurated subsurface soil horizons, and silica and/or clay coatings on the schoepite and metaschoepite crystals, result in little or no contamination risk in this environment, unless land-use or regional climate patterns change. Interpreting environmental health risks by uranium corrosion is best achieved by using a multitude of analytical techniques: combining extraction results (Johnson *et al.*, 2004) with soil-geomorphology, SEM/EDS, XRD, and electron microprobe analyses (Elless and Lee, 2002).

References

- Barnett, M.O., Jardine, P.M., Brooks, S.C., and Selim, H.M. 2000. Adsorption and transport of uranium (VI) in subsurface media. *Soil Sci. Soc. Am. J.* **64**, 908–917.
- Bleise, A., Danesi, P.R., and Burkart, W. 2003. Properties, use and health effects of depleted uranium (DU): A general overview. *J. Environ. Radioact.* **64**, 93–112.
- Buck, B.J. and Van Hoesen, J. 2002. Snowball morphology and SEM analysis of pedogenic gypsum, southern New Mexico, USA. *J. Arid Environ.* **51**, 469–487.
- Buck, B.J., Van Hoesen, J., Khresat, S., and Rawajfih, Z. 2002. Morphology, SEM, and stable isotopic analyses of pedogenic gypsum, USA and Jordan. *transactions of the 17th WCSS. Bangkok, Thailand.* **20**, 451,1–10.
- Chadwick, O.A., Hendricks, D.M., and Nettleton, W.D. 1989. Silicification of holocene soils in northern monitor valley, Nevada. *Soil Sci. Soc. of Am. J.* **53**, 158–164.
- Danesi, P.R., Markowicz, A., China-Cano, E., Burkart, W., Salbu, B., Donohue, D., Ruedenauer, F., Hedberg, M., Vogt, S., Zahradnik, P., and Ciurapinski, A. 2003. Depleted uranium particles in selected Kosovo samples. *J. Environ. Radioact.* **64**, 143–154.
- Driessen, P.M. and Schoorl, R. 1973. Mineralogy and morphology of salt efflorescences on saline soils in the Great Konya Basin, Turkey. *J. Soil Sci.* **24**, 436–442.
- Elless, M.P. Timpson, M.E., and Lee, S.Y. 1997. Concentration of uranium particulates from soils using a novel density-separation technique. *Soil Sci. Soc. of Am. J.* **61**, 626–631.
- Elless, M.P. and Lee, S.Y. 2002. Radionuclide-contaminated soils: A mineralogical perspective for their remediation. In: *Soil Mineralogy with Environmental Applications*, SSSA Book Series, no. 7., pp. 737–763 (J. Dixon and D. Schulze, eds.), Soil Science Society of America, Madison, WI.
- Elless, M.P. and Lee, S.Y. 1998. Uranium solubility of carbonate-rich uranium-contaminated soils. *Water, Air and Soil Poll.* **107**, 147–162.
- Filgueiras, A.V., Lavilla, I., and Bendicho, C. 2002. Chemical sequential extraction for metal partitioning in environmental solid samples. *J. Environ. Monit.* **4**, 823–857.
- Finch, R.J. and Ewing, R.C. 1992. The corrosion of uraninite under oxidizing conditions. *J. Nucl. Mat.* **190**, 133–156.
- Gee, G.W. and Bauder, J.W. 1986. Particle-size analysis. In: *Methods of Soil Analysis Part 1—Physical and Mineralogical Methods*, pp. 383–411, Soil Science Society of America Book Series 5, American Society of Agronomy, Madison, Wisconsin.
- Giannardi, C. and Dominici, D. 2003. Military use of depleted uranium: Assessment of prolonged population exposure. *J. Environ. Radioact.* **64**, 227–236.

- Johnson, W.H., Buck, B.J., Brogonia, H., and Brock, A. 2004. Variations in depleted uranium sorption and solubility with depth in arid soils. *Soil and Sed Contam.* **12**(6), 533–544.
- Keller, L.P., McCarthy, G.J., and Richardson, J.L. 1986. Mineralogy and stability of soil evaporites in North Dakota. *Soil Sci. Soc. Am. J.* **50**, 1069–1071.
- Klein, C. and Hurlbut, C.S. Jr. 1993. *Manual of Mineralogy*, 21st edition, John Wiley and Sons, Inc, New York.
- Langmuir, D. 1978. Uranium solution-mineral equilibrium at low temperatures with applications to sedimentary ore deposits. *Geochim. Cosmochim. Acta* **42**, 547–569.
- Levy, M., Zabielski, M., and Sklover, G.N. 1973. Corrosion Behavior of Depleted Uranium-Titanium and Uranium-Molybdenum Alloys, Army Materials and Mechanics Research Center, Report AMMRC-TR-73-11.
- Meinrath, A., Schneider, P., and Meinrath, G. 2003. Uranium ores and depleted uranium in the environment, with a reference to uranium in the biosphere from the Erzgebirge/Sachsen, Germany. *J. Environ. Radioact.* **64**, 175–193.
- Merkler, D., Buck, B.J., and Wolff, K. 2002. Salts as an Indicator of Hydric Conditions in Las Vegas Wash, Nevada, Annual Meetings Abstracts [CD-ROM]. ASA, CSSA, and SSSSA. Madison, WI.
- Monger, H.C. and Kelly, E.F. 2002. Silica Minerals. In: *Soil Mineralogy with Environmental Applications*, SSSA Book Series, no. 7., pp. 611–636 (J. Dixon and D. Schulze, eds.), Soil Science Society of America, Madison, WI.
- Murakami, T., Ohnuki, T., Isobe, H., and Sato, T. 2001. Field and Laboratory Examination of Uranium Microcrystallization and Its Role in Uranium Transport, Scientific Basis for Nuclear Waste Management XXIV. Sydney, Australia. **663**, 971–977.
- Palmer, R.G. and Troeh, F.R. 1995. *Introductory Soil Science Laboratory Manual*, Oxford University Press, New York, New York.
- Pollanen, R., Ikaheimonen, T. K., Klemola, S., Vartti, V. P., Vesterbacka, K., Ristonmaa, S., Honkamaa, T., Sipila, P., Jokelainen, I., Kosunen, A., Zilliacus, R., Kettunen, M., and Kokkanen, M. 2003. Characterization of projectiles composed of depleted uranium. *J. Environ. Radioact.* **64**, 133–142.
- Rhoades, J.D. 1982. Cation exchange capacity. In: *Methods of Soil Analysis Part 2*, Agron. Monogr. 9, pp. 149–157 (A.L. Page, R.H. Miller, and D.R. Keeney, eds.), Am. Soc. Agron., Madison, WI.
- Schoeneberger, P.J., Wysocki, D.A., Benham, E.C., and Broderson, W.D. 1998. Field book for describing and sampling soils, Natural Resources Conservation Service, USDA, National Soil Survey Center, Lincoln, NE.
- Skarie, R.L., Richardson, J.L., Maianu, A., and Clambey, G.K. 1986. Soil and groundwater salinity along drainage ditches in eastern North Dakota. *J. of Env. Qual.* **15**, 335–340.
- Sowder, A.G., Clark, S.B., and Fjeld, R.A. 1996. The effect of silica and phosphate on the transformation of schoepite to becquerelite and other uranyl phases. *Radiochimica Acta* **74**, 45–49.
- Timpson, M.E., Richardson, J.L., Keller, L.P., and McCarthy, G.J. 1986. Evaporite mineralogy associated with saline seeps in southwestern north Dakota. *Soil Sci. Soc. Am. J.* **50**, 490–493.
- Wiedemann, H.G. and Smykatz-Kloss, W. 1981. Thermal studies on thernardite. *Thermochemica Acta* **50**, 17–29.
- Wronkiewicz, D.J., Bates, J.K., Gerding, T.J., Veleckis, E.T., and Benjamin S. 1992. Uranium release and secondary phase formation during unsaturated testing of UO₂ at 90°C. *J. Nucl. Mat.* **190**, 107–127.